nature communications

Article

https://doi.org/10.1038/s41467-025-65008-3

Droplet surface spontaneous oxidation as a dominant formation pathway of organosulfates in the marine atmosphere

Received: 10 February 2025

Accepted: 2 October 2025

Published online: 19 November 2025

Check for updates

Lin Du[1,2,3,8] ✉, Yaru Song[1,2,8], Jianlong Li[2], Yibei Wan[4], Huan Yu[4], Xueqi Ma[2], Zhaomin Yang[2], Jie Hu[2], Kuanyun Hu[2], Xuxu Gao[5], Qinyi Li[2], Christian George[1,6], Maofa Ge[7] & Kun Li[2] ✉

Organosulfates (OSs) have been widely detected in marine aerosols and have various potential formation pathways in the atmosphere. However, the key formation mechanism of OSs in the marine environment remains unclear. Here, by combining field measurements, laboratory experiments, and model calculations, we suggest that the surface spontaneous oxidation of sea spray aerosol (SSA) particles produces OSs rapidly and is the dominant formation pathway of OSs in the marine atmosphere. SSA microdroplets provide a large surface area for the spontaneous formation of OH radicals, inducing the oxidization of dimethyl sulfide into sulfate (SO_4^{2-}), sulfuric acid, and organic acids, thereby acidifying the droplets. Subsequently, SO_4^{2-} reacts with dissolved alcohols under such acidic conditions to produce OSs. This process is fast enough to be a major source of detected OSs in the aerosol samples collected in the marine atmosphere. This pathway contributes to a global OS production of 13.96 ± 10.99 Tg yr^{-1}, comparable to global isoprene-derived OS production. This study reveals that rapid secondary processes are the main source of OSs in the marine atmosphere and highlights the important role of the droplet surface spontaneous oxidation process in atmospheric chemistry over the ocean.

Marine aerosol particles, particularly those generated directly from the sea surface via bubble bursting (e.g., sea spray aerosol, SSA), significantly influence the climate through solar radiation scattering and absorption, as well as cloud condensation nucleus (CCN) activation, while also exerting a notable impact on coastal air quality[1–4]. These particles can provide microenvironments for heterogeneous and multiphase reactions, thereby altering their chemical composition and affecting their optical, physical, and hygroscopic properties[5,6]. Organic compounds, with a wide range of functionalities, have been proven to be an important component affecting the physicochemical properties of marine aerosol particles. Previous studies primarily focused on quantifying traditional organic tracers and their sources in marine organic aerosol particles[7], along with assessing the percentage contribution of simple organic functional groups in marine aerosol

[1]Qingdao Key Laboratory for Prevention and Control of Atmospheric Pollution in Coastal Cities, School of Environmental Science and Engineering, Shandong University, Qingdao, China. [2]Environment Research Institute, Shandong University, Qingdao, China. [3]State Key Laboratory of Microbial Technology, Shandong University, Qingdao, China. [4]Department of Atmospheric Science, School of Environmental Studies, China University of Geosciences, Wuhan, China. [5]Institute of Marine Science and Technology, Shandong University, Qingdao, China. [6]Universite Claude Bernard Lyon 1, CNRS, IRCELYON, UMR 5256, Villeurbanne, France. [7]State Key Laboratory for Structural Chemistry of Unstable and Stable Species, Beijing National Laboratory for Molecular Sciences (BNLMS), Institute of Chemistry, Chinese Academy of Sciences, Beijing, China. [8]These authors contributed equally: Lin Du, Yaru Song.
✉e-mail: lindu@sdu.edu.cn; kun.li@sdu.edu.cn

particle samples[8]. Focusing on organic matter allows for a deeper understanding of specific subsets of marine aerosol particles, elucidating their role in marine aerosol chemistry and their broader implications for the global climate.

Organosulfates (OSs) are a significant component in marine aerosol particles and profoundly impact their interactions with water and, hence, hygroscopic growth and morphology of aerosol particles[8–10]. A recent ship-based atmospheric study over the Yellow Sea and Bohai Sea found that low-molecular-weight OSs significantly contributed to the composition of marine organic aerosol particles[11]. The formation of OSs may enhance CCN activity of aerosol particles since OSs can affect aerosol particle morphology and reduce surface tension[10]. Moreover, OSs have been shown to undergo oxidative aging in the troposphere, producing highly oxidized species and inorganic sulfates, which can significantly alter radiative forcing[12]. However, the formation pathways of OSs in the marine atmosphere are complex in various studies[13,14].

Laboratory studies have proposed that OSs are formed through various mechanisms[15], including (a) acid-catalyzed epoxide ring-opening[16–18], (b) direct sulfate esterification reactions[19,20], (c) nucleophilic substitution of alcohols with sulfuric acid[21], (d) sulfoxide radical reactions[22,23], and (e) heterogeneous reactions of SO_2[24,25]. However, the dominant pathway in the atmosphere over the ocean remains unknown[11], which requires further analysis in the combination of field and laboratory data.

In this study, we combine field observations and laboratory experiments with high-resolution mass spectroscopy to investigate the formation of OSs in marine aerosol particles comprehensively. A rapid formation of OSs at the aerosol particle surface is observed, indicating that they can be generated spontaneously by secondary processes. This finding improves our understanding of the formation mechanism and impacts of OSs in the marine atmosphere.

Results

OSs in seawater, field marine aerosols, and laboratory marine aerosols

Seawater and aerosol particle samples were collected from the East China Sea and the Indian Ocean (Fig. 1a and Supplementary Table 1). An ultra-high-performance liquid chromatography (UHPLC) coupled with a Q-Exactive hybrid Quadrupole-Orbitrap mass spectrometer was used to obtain MS data and MS^2 spectra for the analysis of OSs in these samples based on ref. 26.

Figure 1b shows the fractional contribution of OSs to total organic compounds detected in these samples. Here, the "fractional contribution" refers to the proportion of OSs relative to the total organic compounds in either seawater or marine aerosol particle samples (Supplementary Text 1). We use the fractional contribution rather than the absolute concentration to quantify OSs because the total organic concentrations in seawater and marine aerosol particles vary significantly. As shown in Fig. 1b and Supplementary Fig. 1, the OS fraction in the organic compounds of the seawater samples from all locations was below the detection limit (0.26 μg L^{-1}). Previous studies on dissolved organic matter in seawater, including both targeted and non-targeted approaches, have not reported the presence of OSs[27,28]. In contrast, a significant presence of OS compounds was found in all the field marine aerosol samples, with the OS fraction ranging from 0.12 ± 0.013 to 0.21 ± 0.020 (Fig. 1b). This significant difference between seawater and marine aerosol particle samples indicates that the OS compounds in the aerosol particle samples are unlikely to originate from the direct transport from seawater to SSA particles. In other words, the OS compounds in marine aerosol particles are from secondary sources, where atmospheric processing is key. However, as shown in Fig. 1c, many OS species are saturated aliphatic OSs (Supplementary Figs. 2, 3), which have been previously considered to originate from primary anthropogenic sources[12,29–31]. Specifically, these assignments were supported by high-resolution mass spectrometry and related molecular characteristics (see "Methods" and Supplementary Fig. 4 for details).

To solve this contradiction, we conducted laboratory-based, in situ SSA generation experiments using seawater collected from the East China Sea and the Indian Ocean (see "Methods"). These laboratory SSA particle samples were collected directly and were processed and analyzed immediately using the same method as the seawater and field aerosol particle samples. Surprisingly, abundant OSs (with a fraction of 0.24 ± 0.024 to 0.39 ± 0.050 in organic compounds) were detected in these SSA particle samples (Fig. 1b). The dominant composition of these laboratory-generated SSA OSs shows similarities to those found in field marine aerosol particles (Fig. 1c and Supplementary Figs. 2, 3), particularly in terms of saturated aliphatic OSs identified in the Indian Ocean (e.g., $C_{12}H_{26}O_4S$, $C_8H_{18}O_4S$). In contrast, differences observed over the East China Sea reflect nearshore anthropogenic influences, consistent with previous findings of enhanced OS abundance in coastal marine aerosols due to continental outflow and regional emissions[32]. It is noteworthy that the OSs detected in SSA particles, as estimated, are improbable as a consequence of enrichment effects (see Supplementary Text 2 for detailed calculations). These results indicate a rapid OS formation process after the SSA particles were generated, as the residence time of these particles from generation to collection was only ~1.5 min (see "Methods").

Notably, the fraction of OSs in organic compounds in the laboratory SSA particle samples was a factor of 1.4–2.9 that of the field marine aerosol particle samples (Fig. 1b). This is likely because atmospheric aging processes can decompose OSs[12] and reduce their fractional contribution to the organic compounds. While aqueous-phase hydrolysis and microbial degradation may also contribute to OS loss under ambient conditions, previous studies suggest that hydrolysis of sulfate esters proceeds slowly in the atmosphere, and that microbial activity in aerosol particles is generally limited[33–35], suggesting that photochemical aging is the primary cause of the observed discrepancy. To verify this hypothesis, we investigated the change in total OS concentration in SSA particles upon photochemical aging by checking the data from our recent study[36], which used an oxidation flow reactor to oxidize the laboratory SSA particles (see Supplementary Text 3, 4 for details). As shown in Supplementary Fig. 5, the total concentration of quantified OS species decreases by approximately 60% as atmospheric aging progresses, and this change mainly occurs within a photochemical age of <2 days. This overall decay trend reflects the influence of heterogeneous OH oxidation in the aerosol phase. Although different OS species may exhibit distinct degradation kinetics depending on their molecular features, the selected compounds are representative of the predominant OS response to photochemical aging[15]. Therefore, despite the structural variability among OS species, the observed degradation trend remains representative of their atmospheric aging processes. Assuming an average photochemical age of the field marine aerosol particles to be 1–2 days[37,38], the difference in OS fraction in laboratory SSA particles and field marine aerosol particles Fig. 1b can be well explained.

Rapid formation processes of OSs

The differences between SSA and seawater that may lead to fast OS formation mainly include two aspects. First, the enrichment of inorganic and organic compounds during SSA particle formation may lead to their higher concentrations in aerosol particles. For example, a recent study showed that the pH of nascent SSA particles could reach ~2, likely due to the enrichment of acidic compounds[39]. In addition, the Kelvin effect in small SSA particles may promote the migration of surface-active organic compounds toward the particle surface due to elevated internal pressure, thereby facilitating interfacial reactions[40,41]. Second, the droplet surface may play a role. SSA particles have a much higher surface-to-volume ratio compared to bulk seawater, where

https://doi.org/10.1038/s41467-025-65008-3

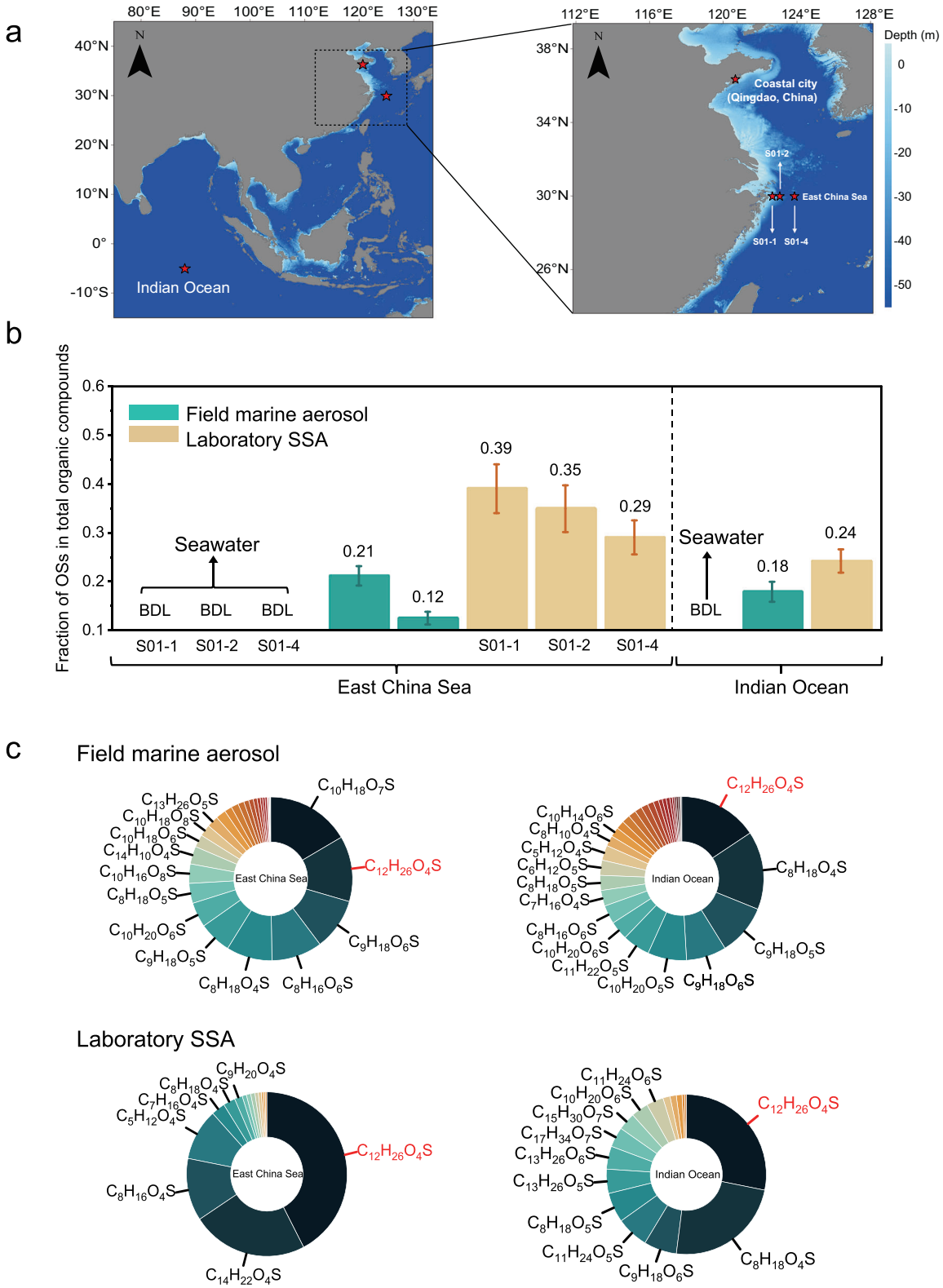

Fig. 1 | The fraction and composition of organosulfates (OSs) in different sampling sites. a Sampling site map, including the East China Sea, Indian Ocean, and coastal city (Qingdao, China), with an enlarged view showing the sampling points in the East China Sea. S01-1, S01-2, and S01-4 are three sampling locations in the East China Sea with different distances to the continent. The global map was created using the ArcGIS Pro 3.0.2 software, and the coastline data were obtained from the Global Self-consistent, Hierarchical, High-resolution Geography Database (GSHHG; https://www.soest.hawaii.edu/pwessel/gshhg/). **b** Fraction of OSs in total organic compounds in seawater, marine aerosols, and sea spray aerosol (SSA), shown in green and yellow for marine aerosols and SSA, respectively. Error bars represent the standard deviation (SD). BDL means "below the detection limit". **c** The OS composition in field marine aerosol and laboratory SSA is shown as the doughnut plots. $C_{12}H_{26}O_4S$, one of the most abundant OS species in particulate matter samples from the East China Sea and Indian Ocean, is highlighted in red.

surface spontaneous oxidation that leads to OH radicals and/or H_2O_2 formation may occur, as previously reported[42–44]. These oxidants may further induce oxidation reactions that form OSs[12,45–50]. Although multiple formation mechanisms may contribute to the presence of OSs in marine aerosols[15,51,52], acid-catalyzed esterification of alcohols with sulfate is likely an important pathway under acidic and precursor-rich conditions.

To reveal the rapid formation mechanism of OSs in the SSA particles, we choose $C_{12}H_{26}O_4S$—a representative OS consistently detected at high abundance in marine and laboratory SSA particles—as an OS proxy to investigate its formation mechanism (Fig. 1c). The structure of $C_{12}H_{26}O_4S$ is relatively simple, with the sulfate ester as the only oxygen-containing functional group and an unsaturation degree of zero for the carbon skeleton. Therefore, the most likely formation pathway of $C_{12}H_{26}O_4S$ is the direct sulfate esterification reactions with C_{12} alcohols (e.g., dodecanols + SO_4^{2-}) under acidic conditions[15,46]. The organic composition of seawater, as shown in Supplementary Fig. 6, was characterized via MS^2 spectra, indicating that alcohols represented 6–31% of the total compound intensity. This value should be interpreted as a relative contribution within the ionizable organic pool, due to potential variations in ionization efficiencies across compound classes. Nonetheless, the relatively high signal intensity associated with alcohol-related fragments suggests that these compounds are non-negligible components of marine organic matter and may play a role in OS formation processes.

These experiments were performed with artificial seawater (ASW) to eliminate the influences of complex components in natural seawater. We produced SSA particles by plunging jetting bulk ASW with or without adding n-dodecanol and analyzed the intensity of $C_{12}H_{26}O_4S$ in the produced SSA particles. As shown in Fig. 2a, no $C_{12}H_{26}O_4S$ was observed in SSA particles from ASW in the absence of alcohol, while the formation of $C_{12}H_{26}O_4S$ was detected in the SSA particles when 3 mg L^{-1} or 0.1 mg L^{-1} n-dodecanol was added to the ASW. The selected concentration serves to elucidate the formation mechanism of OS, rather than to simulate ambient environmental conditions. The extracted ion chromatogram and MS^2 spectra shown in Supplementary Fig. 4 indicate that the $C_{12}H_{26}O_4S$ detected in SSAs particles from seawater and ASW + n-dodecanol have the same structure, which supports our hypothesis that $C_{12}H_{26}O_4S$ is produced from n-dodecanol. In addition, a decrease in SO_4^{2-} concentration was observed in SSA particles following the addition of n-dodecanol to ASW (Fig. 2b), further supporting the OS formation mechanism of alcohol + SO_4^{2-}.

The consumption of SO_4^{2-} in the presence of n-dodecanol exceeded the formation of $C_{12}H_{26}O_4S$ detected in SSA particles. This discrepancy suggests that other potential reaction pathways, such as OH-initiated degradation[15], may influence the fate of precursors and intermediates, further affecting the observed OS yields. These results highlight the importance of microenvironmental conditions at the air-water interface in determining OS production and its transfer efficiency into the aerosol phase.

It is noted that sulfate consumption and OS production were not significant when only n-dodecanol was added to ASW. Therefore, we hypothesize that the spontaneous oxidation of dimethyl sulfide (DMS) at the droplet surface may increase acidity and play an important role in OS formation. DMS is ubiquitous in seawater and the atmosphere above the ocean, and its oxidation processes via OH radicals can produce sulfuric acid[46,53,54]. Sulfuric acid can accelerate the OS formation by enhancing both SO_4^{2-} concentration and particle acidity. To verify this hypothesis, we conducted SSA particle generation experiments by injecting DMS into ASW (ASW + DMS) and injecting DMS and n-dodecanol into ASW (ASW + alcohol + DMS) (see "Methods"). We found that the addition of DMS in ASW indeed enhances the acidity of SSA particles (Supplementary Fig. 7). In addition, as shown in Fig. 2b, the presence of DMS produced a large amount of SO_4^{2-} in SSA particles (~3 times of SSA from ASW only), and a majority of these SO_4^{2-} (~97%) were reacted when n-dodecanol was added as well. The high SO_4^{2-} consumption rate is likely due to the low pH resulting from the production of sulfuric acid, which in turn enhances OS production. As shown in Fig. 2a, the presence of alcohol and DMS led to a significant increase in the production of OSs in SSA particles (~10 times higher than SSA particles in the presence of alcohol only). This significant difference reinforces that the oxidation of DMS, which produces SO_4^{2-} and high acidity, is a key factor for the rapid formation of OSs. It is worth noting that when DMS was completely lost during long-time seawater storage (3 months), the OS formation became negligible. This further emphasizes that DMS and enhanced acidity accelerate OS formation by promoting esterification reactions[12,13,48].

Droplet surface spontaneous oxidation by OH radicals

In the absence of any added oxidants and in the dark, the oxidation of DMS is likely induced by OH radicals produced at the surface of the aerosol droplets. Previous studies have observed the OH radical production at the droplet surface[42–44,55,56]; nevertheless, we performed experiments to measure the OH radicals from this process. We used terephthalic acid (TA) as an OH probe and measured OH radicals by detecting the fluorescent product, 2-hydroxyterephthalic acid (TAOH) (see "Methods" for details). This experiment was conducted with ASW only, without the addition of alcohol or DMS. As shown in Fig. 3a, there was no detectable ·OH in the bulk ASW. However, when we connected a sampling bottle to the SSA simulation chamber, a significant ·OH production was found for the droplets collected in the bottle (e.g., droplet samples in Fig. 3a). Moreover, we also collected the SSA particle samples on filters and found OH radical production in these SSA particle samples (Fig. 3a and Supplementary Fig. 8). Our results confirmed the presence of OH radicals in SSAs particles, and these OH radicals were considered to be the main oxidant in inducing the generation of SO_4^{2-} from DMS.

Based on the above results, we suggest a mechanism for OS generation at the surface of SSA particles (Fig. 3b), where OH radicals are produced by the inherent properties of the air-water interface[42–44,57]. Then, these OH radicals oxidize DMS into sulfur-containing species, predominantly in the gas phase or at the droplet surface, owing to the high volatility and limited aqueous solubility of DMS[58]. DMS can be oxidized by surface OH radicals to form SO_2, dimethyl sulfoxide (DMSO; CH_3SCH_3O), and methane sulfonic acid (MSA; CH_3SO_3H)[47,59]. SO_2 is further oxidized into sulfuric acid in the gas phase in the presence of water vapor[60,61]. Sulfuric acid is dissolved into the aqueous phase and forms SO_4^{2-} and H^+. DMSO and MSA are highly soluble in water, with Henry's law coefficients at 298 K of 10^7 and 10^9 M atm^{-1}, and therefore get into the aqueous phase immediately[46]. In the aqueous phase, the DMSO and MSA are further oxidized into SO_4^{2-} by surface OH radicals[62,63]. At last, the SO_4^{2-} reacts with alcohols in the SSA particles under acidic conditions to form OSs. An increase in surface-to-volume ratio led to a corresponding rise in the relative abundance of $C_{12}H_{26}O_4S$ during identical heterogeneous oxidation experiments (Supplementary Fig. 9), reinforcing the hypothesis that OS formation is a surface-mediated process[64].

The proposed reaction mechanism above shows that OSs are formed through the reactions between alcohols and the products of DMS oxidized by OH radicals at the surface of SSA particles. Therefore, it is expected that the amount of OSs is influenced by alcohol concentration and DMS concentration. To examine the reaction mechanism and investigate the OS production kinetics, we performed a series of experiments by varying alcohol and DMS concentrations (see Supplementary Text 5 and Figs. 10, 11). These parameterizations allow us to extrapolate the obtained OS generation rates to field observations with varying reactant concentrations.

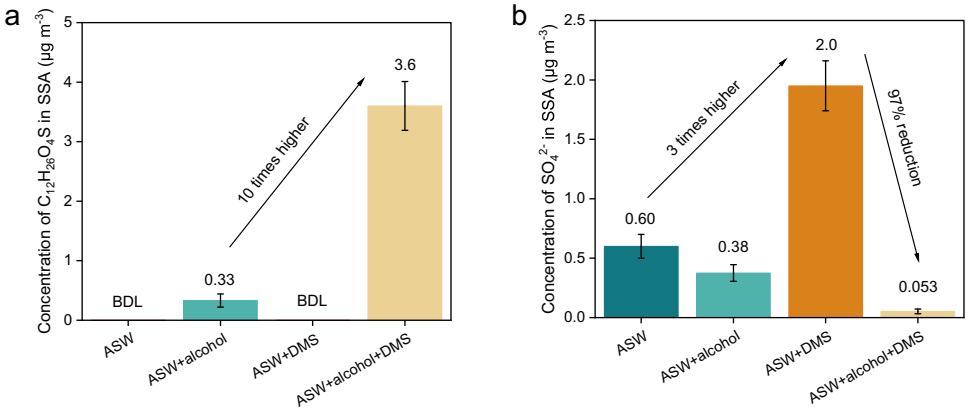

Fig. 2 | Quantification of $C_{12}H_{26}O_4S$ and SO_4^{2-} in sea spray aerosols (SSAs) generated from SSA simulation chamber (n = 3). a Quantification of $C_{12}H_{26}O_4S$ in SSA particle samples generated from artificial seawater (ASW) only, ASW with the presence of n-dodecanol (ASW + alcohol), and ASW with the presence of n-dodecanol and dimethyl sulfide (ASW + alcohol + DMS). Error bars represent the standard deviation (SD). BDL means "below the detection limit". **b** Quantification of SO_4^{2-} in SSAs generated from ASW, ASW + alcohol, ASW + DMS, and ASW + alcohol + DMS. Error bars represent the standard deviation (SD).

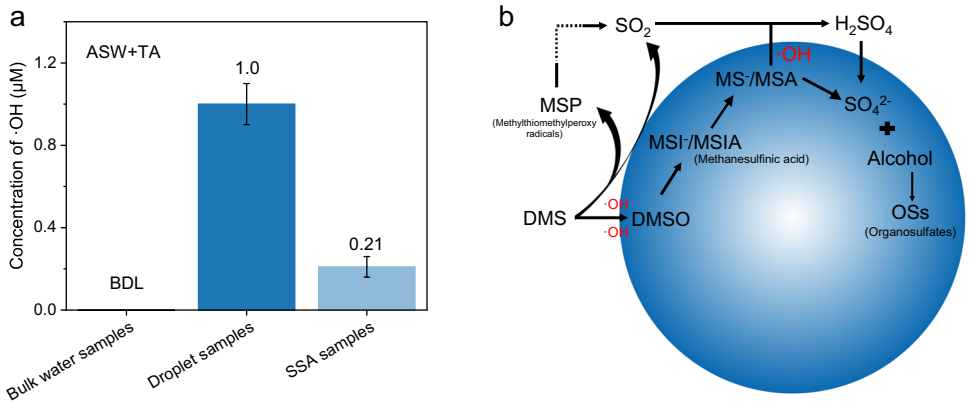

Fig. 3 | ·OH concentration and organosulfates (OSs) formation pathway. a ·OH production measured as the intensity of 2-hydroxyterephthalic acid (TAOH) in bulk water samples, droplets, and sea spray aerosol (SSA) particles. Terephthalic acid (TA) was added as an ·OH scavenger; no alcohol or dimethyl sulfide (DMS) was added in ASW. Error bars represent the standard deviation (SD). BDL means "below detection limit". **b** Reaction mechanism for the formation of OSs initiated by surface OH radicals.

Global OS production estimation and implications

A global-scale mechanistic estimate of OS production from fresh SSA particles is presented, focusing on surface reactions occurring at the air-liquid interface of aerosol droplets. The estimation framework is grounded in laboratory-derived kinetics and employs a rate-limiting step approach to more accurately capture the chemical dynamics controlling OS formation in the marine boundary layer.

The interfacial OS formation mechanism is conceptualized as a two-step process. First, DMS undergoes oxidation at the SSA surface to generate sulfate. Subsequently, sulfate reacts with alcohols to form OSs via esterification. Kinetic analysis based on experimentally determined rate constants, combined with representative atmospheric conditions, reveals that the initial sulfate formation step is substantially slower than the subsequent esterification reaction. This step is governed by both the ambient DMS concentration and the surface area density (SAD) of SSA particles[65–68]. Given the significant disparity in reaction rates, sulfate formation acts as the rate-limiting step and thus constrains the overall OS production potential (see "Methods" for details).

To quantify the global OS production rate from this surface pathway, the monthly gridded outputs from a global chemistry-climate model (Community Atmosphere Model with Chemistry, CAM-Chem) for the year 2019 were employed. The model description and setup are presented in "Methods". The input fields include the atmospheric mixing ratio of DMS and the surface area density of SSA particles, with a horizontal resolution of 0.9° latitude × 1.25° longitude. Calculations were restricted to the planetary boundary layer (PBL), where freshly emitted SSA particles are most abundant and surface reactions are most active. For each grid cell, the sulfate formation rate was computed based on local DMS and SAD values, and the results were vertically integrated using model-derived layer thickness and air density. The integrated mass fluxes were subsequently aggregated globally to yield the total OS production.

The model results in Fig. 4 reveal pronounced geographic heterogeneity in OS production associated with SSA surface chemistry. Higher OS formation rates are observed over biologically active ocean regions, such as the Southern Ocean, where DMS emissions and SSA surface area densities are elevated (see Supplementary Figs. 12–15 for details). These spatial patterns suggest that OS production via the surface oxidation pathway is predominantly driven by the co-occurrence of enhanced DMS availability and abundant SSA surface area. The OS production rate via this pathway was estimated to be between 1×10^{-10} to 1×10^{-5} μg m^{-3} s^{-1}. By integrating this rate over the global marine boundary layer, the total global OS production flux attributed to this mechanism is estimated at 13.96 ± 10.99 Tg yr^{-1}. This places it within the same magnitude as previously reported global

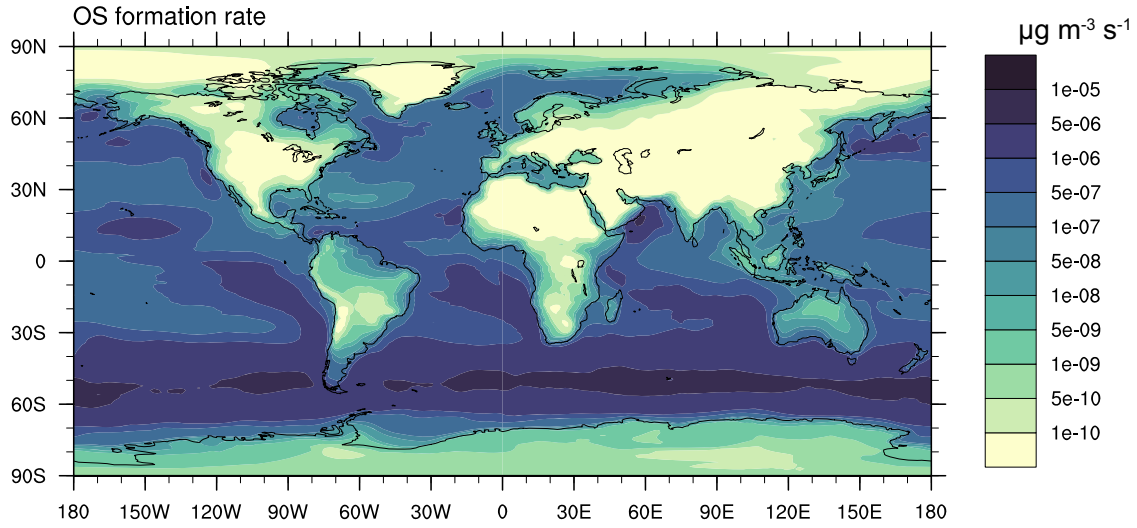

Fig. 4 | Global distribution of organosulfate (OS) production rate (μg m^{-3} s^{-1}) from the droplet surface oxidation process averaged within the boundary layer for the year 2019. The base map was rendered with the NCAR Command Language software Version 6.6.2 https://doi.org/10.5065/D6WD3XH5.

estimates for isoprene-derived OS production (2.8–21 Tg yr^{-1})[15]. Isoprene is an essential component in biogenic emissions and has long been recognized as a dominant precursor of OSs in continental regions[69]. Based on the model estimation results, we suggest that OS formation from DMS oxidation over ocean surfaces may represent a comparably important source in marine environments. These findings underscore the potentially significant, yet previously overlooked, contribution of ocean-derived interfacial processes to the global OS budget.

Discussion

Understanding the sources and generation mechanisms for OSs has significant implications for marine biogeochemical cycles, particularly those involving sulfur compounds, providing insights into the complex interactions between marine ecosystems and the atmosphere[11,15,31]. This study reveals a rapid formation mechanism of OSs at the SSA surface, thereby updating our understanding of their marine atmospheric sources. Building on this foundation, we estimated the global OS production from this pathway to be 13.96 ± 10.99 Tg yr^{-1}, which represents a significant source of OS formation in the marine atmosphere. The observed rapid formation of OSs highlights the role of droplet surface spontaneous oxidation processes in the marine atmosphere, with significant implications for understanding related sulfur-containing species in marine atmospheric chemistry. Taken together, the findings of this study advance our understanding of OS formation in the marine atmosphere and have broader implications for atmospheric chemistry, climate, and marine biogeochemistry.

Methods

Sampling site and experimental setup

A total of 18 seawater samples were collected during the cruise, comprising 9 from the East China Sea, 6 from the Indian Ocean, and 3 from a coastal city (Qingdao, China; Supplementary Table 1 and Fig. 1). Seawater samples were collected from a depth of five meters using a centrifugal pump, filtered through 0.2 μm membranes, and stored at 4 °C in the dark in pre-cleaned HDPE bottles. All samples were analyzed within one month. This procedure follows established methods for preserving dissolved organic matter in seawater[70]. Marine aerosol particle samples were collected aboard using prebaked quartz fiber filters provided by Pall Life Sciences, employing a high-volume sampler with a total suspended particle inlet operated at a flow rate of 1.05 m^3 min^{-1}. The sampler, which collects particles with aerodynamic diameters typically less than 50 μm[71], was placed on the upper deck (~8 m above sea level) to minimize contamination from ship exhaust gases. Filter samples were only collected when the ship was sailing, ensuring representative sampling, and the total sampling time was 24 h. To monitor and account for any ambient contamination, field blank samples were collected with the instrument pump turned off, also over 24 h. All filters were pre-baked at 500 °C for 4 h in a muffle furnace to remove organic contaminants before sampling. After sampling, the filters were placed in filter holders and stored frozen at −20 °C in the dark until analysis.

A jet-based SSA simulation chamber (30 cm × 20 cm × 40 cm) made up of stainless steel was designed to mimic SSA particle generation filled with 9 L seawater from the East China Sea and the Indian Ocean (Supplementary Fig. 16). When necessary, in artificial seawater (ASW) experiments, DMS was diffused into the SSA chamber through the "air" port using a syringe pump at a fixed concentration, while the alcohol was directly injected into the ASW. Details of the chamber were provided in our previous papers[72–74]. A flow of 10 L min^{-1} zero air was drifting through the chamber above the seawater surface, to carry the SSA particles through the Nafion drying tube (MD-700-06S-3, Perma Pure, USA) onto a 47 mm quartz fiber filter (QFF, 1851-025, Waterman, UK) placed in a stainless-steel inline filter holder (Sartorius 16254, Sartorius Stedim Biotech GmbH, Germany) with a flow rate of 9 L min^{-1}. The average lifetime of these SSA particles from generation to collection was estimated to be ~1.5 min based on the chamber volume and air flow rate. Particle size distribution was measured in situ using a scanning mobility particle sizer during the spraying process (Supplementary Fig. 17), consisting of a differential mobility analyzer (DMA, Model 3081, TSI, USA) and a condensation particle counter (CPC, Model 3776, TSI, USA)[75].

Quantification of organic compounds

Field and laboratory filter samples were dissolved and filtered through a 0.22 μm pore size PTFE syringe filter (Millipore). The solution was loaded on a SPE cartridge (Oasis HLB, Waters, USA), and concentrated to near dryness under a gentle stream of nitrogen. The concentrated samples were reconstituted with 200 μL methanol (Optima® LC-MS grade, Fisher Scientific) and analyzed by UHPLC coupled with a Q-Exactive hybrid Quadrupole-Orbitrap mass spectrometer (Thermo Scientific, Bremen, Germany). Likewise, 20 mL of the seawater samples were first filtered and then processed using the same SPE protocol to remove inorganic salts and enrich organic compounds. The eluents

were subsequently concentrated and reconstituted with 200 μL methanol for UHPLC-MS analysis.

HPLC separation was performed using a Hypersil Gold C18 column (3.0 μm particle size, 3 × 150 mm, Thermo Fisher) with a flow rate of 300 μL min^{-1}. The binary mobile phase consisted of 0.1% formic acid (A) and methanol (B). SSA extracts were conducted using a gradient elution program: initially set to 5% eluent B over the first 4 min, the concentration of eluent B was increased linearly to 100% in 72 min, held for 3 min, then it was decreased from 100% to 5% in 0.5 min, and finally kept at 5% for 12.5 min to recondition the column. The following parameters were set for the optimal operation of UHPLC Q-Extractive hybrid Quadrupole-Orbitrap mass spectrometer: spray voltage (+), 3.2 kV; spray voltage (−), 2.6 kV; capillary temperature, 350 °C. All data were recorded and processed using MZmine version 2.33. Details of MZmine settings and acquisition of MS spectra have been described previously[26], and only a brief description is given here. All the detected formulas in the range of $C_{1\text{-}50}H_{1\text{-}100}O_{1\text{-}40}N_{0\text{-}5}S_{0\text{-}2}$ were selected with a mass tolerance of ±5 ppm, and a chromatographic peak area of more than 10^5. Based on the data analysis workflow for nontarget tandem high-resolution mass spectrometry proposed by Wan et al.[26], data with a sample/blank ratio of more than 100 were exported for MS^2 processing. A series of surrogate standards were employed to semi-quantify the $[M\text{-}H]^-$ molecular ions, with detailed information on quantification procedures and structural assignment provided in Supplementary Table 2 and Text 6. Details regarding ionization efficiency, associated quantification uncertainties, and calibration parameters (slope, intercept, and correlation coefficients) of the surrogate standards employed in this study are presented in the Supplementary Table 3 and Text 7.

Quantification of ·OH

The ·OH formed at the droplet surface was quantified with terephthalic acid (TA). TA reacts with ·OH to form 2-hydroxyterephthalic acid (TAOH) with a production yield of 0.315[57]. TAOH, as a fluorescent compound, can be quantified using a fluorescence spectrometer equipped with quartz cuvettes with a 1 cm path length. The excitation wavelength (Ex) was set at 310 nm, and the emission wavelength (Em) was recorded in the range of 380–480 nm at a speed rate of 200 nm min^{-1}, with increments of 5 nm steps[43]. The data were exported from the software EzSpec. The experiments were performed with added TA as an OH scavenger. The intensity of TAOH in ASW, SSA droplets, and dried SSA aerosol particles was calculated as ·OH production. Specifically, the droplet samples were collected using the SSA simulation chamber through the "excess air" port before entering the SSA particle sampler, as shown in Supplementary Fig. 16.

Additional measurements

To get details about the morphology of SSA particles (see Supplementary Fig. 18), particles collected onto copper grid films (T11023, Tianld, China) using a single particle sampler (DKL-2, Genstar electronic technology Co., Ltd, China) were analyzed by transmission electron microscope (TEM, FEI Tecnai G2 F20, Thermo Fisher Scientific, USA)[76]. Water-soluble inorganic ions (Na^+, SO_4^{2-}) were quantified by ion chromatographs (Dionex ICS-600, Thermo Fisher Scientific, USA) coupled with conductivity detection[77] to calculate the enrichment factors of functional group categories (see Supplementary Text 8 and Fig. 19). The extract solution was injected into the analytical column by a six-way valve mounted with a loop of 10 μL.

Kinetic framework of OS formation via SSA surface reactions

The formation of OSs via freshly emitted SSAs is represented by a two-step surface-mediated chemical mechanism. The proposed pathway involves the in-situ oxidation of DMS at the air-water interface of SSA droplets to produce sulfate species, followed by esterification reactions between the sulfate and alcohols present in the marine atmosphere. The overall mechanism is described as follows:

Step 1: DMS oxidation at the SSA surface

$$DMS(g) + OH \rightarrow SO_4^{2-}$$

Step 2: Esterification of sulfate with alcohol

$$SO_4^{2-} + ROH \xrightarrow{H^+} ROSO_3H$$

Based on laboratory-derived kinetic measurements, the rates of these two steps can be expressed as Eqs. (1) and (2):

$$\frac{d[SO_4^{2-}]}{dt} = k_1 \times [DMS] \times SAD \quad (1)$$

where $k_1 = 1.31 \times 10^3$ g m^{-2} s^{-1}, [DMS] is the atmospheric mixing ratio of DMS (ppb), and SAD is the SSA surface area density (cm^{-2} cm^{-3}).

$$\frac{d[OS]}{dt} = k_2 \times \left[SO_4^{2-}\right] \times [ROH] \quad (2)$$

where $k_2 = 3.36 \times 10^5$ m^3 g^{-1} s^{-1}, [SO_4^{2-}] and [ROH] represent the ambient concentrations of sulfate and alcohol (μg m^{-3}), respectively. Details on the derivation of the rate constants k_1 and k_2 can be found in Supplementary Text 9.

Using representative atmospheric concentrations reported in the literature—namely [DMS] = 0.3 ppb[65,67], [SO_4^{2-}] = 3 μg m^{-3}[78,79], [ROH] = 1 ng m^{-3}[80–82], and SAD = 10 μm^2 cm^{-3}[66,68]—the comparison of the two rate expressions reveals that the formation rate of sulfate (1.31×10^{-11} g m^{-3} s^{-1}) is substantially slower than the subsequent esterification step (1.01×10^{-9} g m^{-3} s^{-1}). This result indicates that the initial DMS oxidation process is the rate-limiting step in the overall OS formation pathway. As such, the global OS production flux was estimated based on the sulfate production rate, which closely approximates the actual OS formation via this surface-driven mechanism, given the high conversion efficiency observed in our experiments.

Global model framework and data inputs

To estimate the global production of OS via SSA surface oxidation, the sulfate formation rate equation was applied globally using meteorological and chemical fields from a global chemistry-climate model (CAM-Chem) that has been widely used to conduct global DMS- and SSA-related investigations[49,83]. Here, we follow the model setup in Li et al.[83] and run the model from January 2018 to December 2019, using only the simulated data (monthly average DMS mixing ratios and SSA surface area densities) in 2019 for analysis. The data had a spatial resolution of 0.9° latitude × 1.25° longitude. The simulated DMS and SSA surface area concentrations show good agreement with available field observations, supporting the reliability of the model outputs[65–68]. A detailed comparison between simulated and observed values is provided in the Supplementary Tables 4 and 5.

Given that SSA surface reactions predominantly occur in the lower troposphere, calculations were restricted to the PBL. For each grid cell, the sulfate production rate was computed as Eq. (3):

$$\left(\frac{d\left[SO_4^{2-}\right]}{dt}\right)_{ijk} = k_1 \times [DMS]_{ijk} \times SAD_{ijk} \quad (3)$$

The resulting production rate (in μg m^{-3} s^{-1}) was multiplied by the model-derived layer thickness dz_{ijk} to yield a vertically integrated flux (μg m^{-2} s^{-1}). The layer thickness was calculated from hydrostatic pressure and modeled air density fields. Global OS mass fluxes were then

computed by multiplying the vertically integrated rate with the corresponding surface area of each grid cell, and summing across all cells to obtain global monthly and annual totals.

To evaluate the uncertainty in our global estimate, we conducted an uncertainty analysis based on error propagation from the rate-limiting step of sulfate formation. We considered uncertainties of ±20% for each of the three key experimental parameters—DMS concentration, SSA surface area density, and measured sulfate formation rate—yielding a combined experimental uncertainty of ±34.6%. Additional uncertainty of ±50% from model integration and global scaling was incorporated to account for potential variability in grid-level inputs and vertical integration. The resulting total propagated uncertainty was ±78.7%, leading to a global OS formation flux of 13.96 ± 10.99 Tg yr^{-1}. A detailed description of this calculation is provided in Supplementary Text 10.

Data availability

The data used in this study are available in the Zenodo database under accession code https://doi.org/10.5281/zenodo.16990475[84].

References

1. Mayer, K. J., Sauer, J. S., Dinasquet, J. & Prather, K. A. CAICE studies: insights from a decade of ocean-atmosphere experiments in the laboratory. *Acc. Chem. Res.* **53**, 2510–2520 (2020).
2. Quinn, P. K., Collins, D. B., Grassian, V. H., Prather, K. A. & Bates, T. S. Chemistry and related properties of freshly emitted sea spray aerosol. *Chem. Rev.* **115**, 4383–4399 (2015).
3. van Pinxteren, M. et al. Amino acids, carbohydrates, and lipids in the tropical oligotrophic Atlantic Ocean: sea-to-air transfer and atmospheric in situ formation. *Atmos. Chem. Phys.* **23**, 6571–6590 (2023).
4. Xu, W. et al. Sea spray as an obscured source for marine cloud nuclei. *Nat. Geosci.* **15**, 282–286 (2022).
5. Abbatt, J. P. D. & Ravishankara, A. R. Opinion: atmospheric multiphase chemistry–past, present, and future. *Atmos. Chem. Phys.* **23**, 9765–9785 (2023).
6. Bertram, T. H., Cochran, R. E., Grassian, V. H. & Stone, E. A. Sea spray aerosol chemical composition: elemental and molecular mimics for laboratory studies of heterogeneous and multiphase reactions. *Chem. Soc. Rev.* **47**, 2374–2400 (2018).
7. Fu, P., Kawamura, K. & Miura, K. Molecular characterization of marine organic aerosols collected during a round-the-world cruise. *J. Geophys. Res.* **116**, D13302 (2011).
8. Lewis, S. L. et al. Seasonal differences in submicron marine aerosol particle organic composition in the North Atlantic. *Front. Mar. Sci.* **8**, 720208 (2021).
9. Estillore, A. D. et al. Water uptake and hygroscopic growth of organosulfate aerosols. *Environ. Sci. Technol.* **50**, 4259–4268 (2016).
10. Riva, M. et al. Increasing isoprene epoxydiol-to-inorganic sulfate aerosol ratio results in extensive conversion of inorganic sulfate to organosulfur forms: implications for aerosol physicochemical properties. *Environ. Sci. Technol.* **53**, 8682–8694 (2019).
11. Wang, Y. et al. Important roles and formation of atmospheric organosulfates in marine organic aerosols: influence of phytoplankton emissions and anthropogenic pollutants. *Environ. Sci. Technol.* **57**, 10284–10294 (2023).
12. Ng, S. I. M. et al. Chemical transformation of a long-chain alkyl organosulfate via heterogeneous OH oxidation: a case study of sodium dodecyl sulfate. *Environ. Sci. Atmos.* **2**, 1060–1075 (2022).
13. Cooke, M. E. et al. Organosulfate formation in proxies for aged sea spray aerosol: reactive uptake of isoprene epoxydiols to acidic sodium sulfate. *ACS Earth Space Chem.* **6**, 2790–2800 (2022).
14. Kanellopoulos, P. G. et al. $PM_{2.5}$-bound organosulfates in two Eastern Mediterranean cities: the dominance of isoprene organosulfates. *Chemosphere* **297**, 134103 (2022).
15. Brüggemann, M. et al. Organosulfates in ambient aerosol: state of knowledge and future research directions on formation, abundance, fate, and importance. *Environ. Sci. Technol.* **54**, 3767–3782 (2020).
16. Shalamzari, M. S. et al. Characterization of polar organosulfates in secondary organic aerosol from the unsaturated aldehydes 2-*E*-pentenal, 2-*E*-hexenal, and 3-*Z*-hexenal. *Atmos. Chem. Phys.* **16**, 7135–7148 (2016).
17. Shang, J. et al. SO_2 uptake on oleic acid: a new formation pathway of organosulfur compounds in the atmosphere. *Environ. Sci. Technol. Lett.* **3**, 67–72 (2016).
18. Zhang, H. et al. Organosulfates as tracers for secondary organic aerosol (SOA) formation from 2-methyl-3-Buten-2-ol (MBO) in the atmosphere. *Environ. Sci. Technol.* **46**, 9437–9446 (2012).
19. Iinuma, Y. et al. Evidence for the existence of organosulfates from β-pinene ozonolysis in ambient secondary organic aerosol. *Environ. Sci. Technol.* **41**, 6678–6683 (2007).
20. Perri, M. J., Lim, Y. B., Seitzinger, S. P. & Turpin, B. J. Organosulfates from glycolaldehyde in aqueous aerosols and clouds: laboratory studies. *Atmos. Environ.* **44**, 2658–2664 (2010).
21. Liggio, J. & Li, S. M. Organosulfate formation during the uptake of pinonaldehyde on acidic sulfate aerosols. *Geophys. Res. Lett.* **33**, L13808 (2006).
22. Wach, P. et al. Radical oxidation of methyl vinyl ketone and methacrolein in aqueous droplets: characterization of organosulfates and atmospheric implications. *Chemosphere* **214**, 1–9 (2019).
23. Rudzinski, K. J., Gmachowski, L. & Kuznietsova, I. Reactions of isoprene and sulphoxy radical-anions–a possible source of atmospheric organosulphites and organosulphates. *Atmos. Chem. Phys.* **9**, 2129–2140 (2009).
24. Passananti, M. et al. Organosulfate formation through the heterogeneous reaction of sulfur dioxide with unsaturated fatty acids and long-chain alkenes. *Angew. Chem. Int. Ed.* **55**, 10336–10339 (2016).
25. Ye, J., Abbatt, J. P. D. & Chan, A. W. H. Novel pathway of SO_2 oxidation in the atmosphere: reactions with monoterpene ozonolysis intermediates and secondary organic aerosol. *Atmos. Chem. Phys.* **18**, 5549–5565 (2018).
26. Wan, Y. et al. Nontarget tandem high-resolution mass spectrometry analysis of functionalized organic compounds in atmospherically relevant samples. *Environ. Sci. Technol. Lett.* **9**, 1022–1029 (2022).
27. Alygizakis, N., Giannakopoulos, T., Tauhomaidis, N. S. & Slobodnik, J. Detecting the sources of chemicals in the Black Sea using non-target screening and deep learning convolutional neural networks. *Sci. Total Environ.* **847**, 157554 (2022).
28. Gandar, A. et al. Targeted and untargeted discovery of UV filters and emerging contaminants with environmental risk assessment on the Northwestern Mediterranean coast. *Mar. Pollut. Bull.* **212**, 117567 (2025).
29. Cochran, R. E. et al. Analysis of organic anionic surfactants in fine and coarse fractions of freshly emitted sea spray aerosol. *Environ. Sci. Technol.* **50**, 2477–2486 (2016).
30. Hettiyadura, A. P. S. et al. Qualitative and quantitative analysis of atmospheric organosulfates in Centreville, Alabama. *Atmos. Chem. Phys.* **17**, 1343–1359 (2017).
31. Ng, S. I. M. & Chan, M. N. Beyond the formation: unveiling the atmospheric transformation of organosulfates via heterogeneous OH oxidation. *Chem. Commun.* **59**, 13919–13938 (2023).
32. Bao, H., Niggemann, J., Luo, L., Dittmar, T. & Kao, S.-J. Molecular composition and origin of water-soluble organic matter in marine aerosols in the Pacific off China. *Atmos. Environ.* **191**, 27–35 (2018).

33. Darer, A. I., Cole-Filipiak, N. C., O'Connor, A. E. & Elrod, M. J. Formation and stability of atmospherically relevant isoprene-derived organosulfates and organonitrates. *Environ. Sci. Technol.* **45**, 1895–1902 (2011).
34. Bondy, A. L. et al. Isoprene-derived organosulfates: vibrational mode analysis by Raman spectroscopy, acidity-dependent spectral modes, and observation in individual atmospheric particles. *J. Phys. Chem. A* **122**, 303–315 (2018).
35. Collins, D. B. et al. Impact of marine biogeochemistry on the chemical mixing state and cloud-forming ability of nascent sea spray aerosol. *J. Geophys. Res. Atmos.* **118**, 8553–8565 (2013).
36. Ma X. et al. Molecular characteristics of sea spray aerosols during aging with the participation of marine volatile organic compounds. *Sci. Total Environ.* **954**, 176380 (2024).
37. Che, H. et al. Cloud processing and weeklong ageing affect biomass burning aerosol properties over the southeastern Atlantic. *Commun. Earth Environ.* **3**, 182 (2022).
38. Tang, Y. et al. Multiscale simulations of tropospheric chemistry in the eastern Pacific and on the U.S. West Coast during spring 2002. *J. Geophys. Res. Atmos.* **109**, D23S11 (2004).
39. Angle, K. J. et al. Acidity across the interface from the ocean surface to sea spray aerosol. *Proc. Natl. Acad. Sci. Usa.* **118**, e2018397118 (2021).
40. Petters, S. S. Constraints on the role of Laplace pressure in multiphase reactions and viscosity of organic aerosols. *Geophys. Res. Lett.* **49**, e2022GL098959 (2022).
41. Tumminello, P. R. et al. Size-dependent nascent sea spray aerosol bounce fractions and estimated viscosity: the role of divalent cation enrichment, surface tension, and the Kelvin effect. *Environ. Sci. Technol.* **58**, 19666–19678 (2024).
42. Angelaki, M., Carreira Mendes Da Silva, Y., Perrier, S. & George, C. Quantification and mechanistic investigation of the spontaneous H_2O_2 generation at the interfaces of salt-containing aqueous droplets. *J. Am. Chem. Soc.* **146**, 8327–8334 (2024).
43. Li, K. et al. Spontaneous dark formation of OH radicals at the interface of aqueous atmospheric droplets. *Proc. Natl. Acad. Sci. USA.* **120**, e2220228120 (2023).
44. Lee, J. K. et al. Spontaneous generation of hydrogen peroxide from aqueous microdroplets. *Proc. Natl. Acad. Sci. USA.* **116**, 19294–19298 (2019).
45. Chen, Y. et al. Heterogeneous hydroxyl radical oxidation of isoprene-epoxydiol-derived methyltetrol sulfates: plausible formation mechanisms of previously unexplained organosulfates in ambient fine aerosols. *Environ. Sci. Technol. Lett.* **7**, 460–468 (2020).
46. Fung, K. M. et al. Exploring dimethyl sulfide (DMS) oxidation and implications for global aerosol radiative forcing. *Atmos. Chem. Phys.* **22**, 1549–1573 (2022).
47. Hoffmann, E. H., Heinold, B., Kubin, A., Tegen, I. & Herrmann, H. The importance of the representation of DMS oxidation in global chemistry-climate simulations. *Geophys. Res. Lett.* **48**, e2021GL094068 (2021).
48. Kwong, K. C., Chim, M. M., Davies, J. F., Wilson, K. R. & Chan, M. N. Importance of sulfate radical anion formation and chemistry in heterogeneous OH oxidation of sodium methyl sulfate, the smallest organosulfate. *Atmos. Chem. Phys.* **18**, 2809–2820 (2018).
49. Veres, P. R. et al. Global airborne sampling reveals a previously unobserved dimethyl sulfide oxidation mechanism in the marine atmosphere. *Proc. Natl. Acad. Sci. USA* **117**, 4505–4510 (2020).
50. Xu, R. et al. Chemical transformation of α-pinene-derived organosulfate via heterogeneous OH oxidation: implications for sources and environmental fates of atmospheric organosulfates. *Atmos. Chem. Phys.* **22**, 5685–5700 (2022).
51. Surratt, J. D. et al. Organosulfate formation in biogenic secondary organic aerosol. *J. Phys. Chem. A* **112**, 8345–8378 (2008).
52. Surratt, J. D. et al. Evidence for organosulfates in secondary organic aerosol. *Environ. Sci. Technol.* **41**, 517–527 (2006).
53. Wohl, C. et al. Marine emissions of methanethiol increase aerosol cooling in the Southern Ocean. *Sci. Adv.* **10**, eadq2465 (2024).
54. Yan, J. et al. Influence on the conversion of DMS to MSA and SO_4^{2-} in the Southern Ocean, Antarctica. *Atmos. Environ.* **233**, 117611 (2020).
55. Angelaki, M., d'Erceville, J., Donaldson, D. J. & George, C. pH affects the spontaneous formation of H_2O_2 at the air–water interfaces. *J. Am. Chem. Soc.* **146**, 25889–25893 (2024).
56. Qiu, L. & Cooks, R. G. Spontaneous oxidation in aqueous microdroplets: water radical cation as primary oxidizing agent. *Angew. Chem. Int. Ed.* **63**, e202400118 (2024).
57. Gonzalez, D. H., Kuang, X. M., Scott, J. A., Rocha, G. O. & Paulson, S. E. Terephthalate probe for hydroxyl radicals: Yield of 2-hydroxyterephthalic acid and transition metal interference. *Anal. Lett.* **51**, 2488–2497 (2018).
58. Jou, F. Y., Mather, A. E. & Schmidt, K. A. G. Solubility of dimethyl sulfide in water. *Ind. Eng. Chem. Res.* **64**, 6180–6187 (2025).
59. Ye, Q. et al. Product distribution, kinetics, and aerosol formation from the OH oxidation of dimethyl sulfide under different RO_2 regimes. *Atmos. Chem. Phys.* **22**, 16003–16015 (2022).
60. Emmons, L. K. et al. The chemistry mechanism in the Community Earth System Model version 2 (CESM2). *J. Adv. Model. Earth Syst.* **12**, e2019MS001882 (2020).
61. Lamarque, J.-F. et al. CAM-chem: description and evaluation of interactive atmospheric chemistry in the Community Earth System Model. *Geosci. Model Dev.* **5**, 369–411 (2012).
62. Breider, T. J. et al. Impact of BrO on dimethylsulfide in the remote marine boundary layer. *Geophys. Res. Lett.* **37**, L02807 (2010).
63. Yang, Y. et al. Global source attribution of sulfate concentration and direct and indirect radiative forcing. *Atmos. Chem. Phys.* **17**, 8903–8922 (2017).
64. Zhang, W., Issa, K., Tang, T. & Zhang, H. Role of hydroperoxyl radicals in heterogeneous oxidation of oxygenated organic aerosols. *Environ. Sci. Technol.* **58**, 4727–4736 (2024).
65. Park, K. T. et al. Dimethyl sulfide-induced increase in cloud condensation nuclei in the Arctic atmosphere. *Glob. Biogeochem. Cycles* **35**, e2021GB006969 (2021).
66. Moore, K. A. et al. Estimation of sea spray aerosol surface area over the southern ocean using scattering measurements. *J. Geophys. Res. Atmos.* **127**, e2022JD037009 (2022).
67. Mahajan, A. S. et al. Quantifying the impacts of an updated global dimethyl sulfide climatology on cloud microphysics and aerosol radiative forcing. *J. Geophys. Res. Atmos.* **120**, 2524–2536 (2015).
68. Wang, Y. et al. An updated aerosol simulation in the Community Earth System Model (v2.1.3): dust and marine aerosol emissions and secondary organic aerosol formation. *Geosci. Model Dev.* **17**, 7995–8021 (2024).
69. Surratt, J. D. et al. Evidence for organosulfates in secondary organic aerosol. *Environ. Sci. Technol.* **41**, 517–527 (2007).
70. Fourrier, P., Dulaquais, G. & Riso, R. Influence of the conservation mode of seawater for dissolved organic carbon analysis. *Mar. Environ. Res.* **181**, 105754 (2022).
71. Krug, J. D. et al. Revisiting the size selective performance of EPA's high-volume total suspended particulate matter (Hi-Vol TSP) sampler. *Aerosol Sci. Technol.* **51**, 868–878 (2017).
72. Liu, L., Du, L., Xu, L., Li, J. & Tsona, N. T. Molecular size of surfactants affects their degree of enrichment in the sea spray aerosol formation. *Environ. Res.* **206**, 112555 (2022).
73. Song, Y., Li, J., Tsona, N. T., Liu, L. & Du, L. Enrichment of short-chain organic acids transferred to submicron sea spray aerosols. *Sci. Total Environ.* **851**, 158122 (2022).
74. Song, Y., Li, J., Tsona Tchinda, N., Li, K. & Du, L. Role of sea spray aerosol at the air–sea interface in transporting aromatic acids to the atmosphere. *Atmos. Chem. Phys.* **24**, 5847–5862 (2024).

75. O'Dowd, C. D. et al. Biogenically driven organic contribution to marine aerosol. *Nature* **431**, 676–680 (2004).
76. Li, W. et al. Microscopic evidence for phase separation of organic species and inorganic salts in fine ambient aerosol particles. *Environ. Sci. Technol.* **55**, 2234–2242 (2021).
77. Hu, J. et al. Underestimated role of sea surface temperature in sea spray aerosol formation and climate effects. *npj Clim. Atmos. Sci.* **7**, 273 (2024).
78. Sarin, M., Kumar, A., Srinivas, B., Sudheer, A. K. & Rastogi, N. Anthropogenic sulphate aerosols and large Cl-deficit in marine atmospheric boundary layer of tropical Bay of Bengal. *J. Atmos. Chem.* **66**, 1–10 (2011).
79. Ooki, A., Miura, K. & Uematsu, M. The increase of biogenic sulfate aerosol and particle number in marine atmosphere over the northwestern North Pacific. *J. Oceanogr.* **59**, 799–807 (2003).
80. Kawamura, K., Hoque, M. M. M., Bates, T. S. & Quinn, P. K. Molecular distributions and isotopic compositions of organic aerosols over the western North Atlantic: dicarboxylic acids, related compounds, sugars, and secondary organic aerosol tracers. *Org. Geochem.* **113**, 229–238 (2017).
81. Kang, M. et al. Influence of continental organic aerosols to the marine atmosphere over the East China Sea: Insights from lipids, PAHs and phthalates. *Sci. Total Environ.* **607–608**, 339–350 (2017).
82. Boreddy, S. K. R., Haque, M. M., Kawamura, K., Fu, P. & Kim, Y. Homologous series of n-alkanes (C_{19}-C_{35}), fatty acids (C_{12}-C_{32}) and n-alcohols (C_8-C_{30}) in atmospheric aerosols from central Alaska: molecular distributions, seasonality and source indices. *Atmos. Environ.* **184**, 87–97 (2018).
83. Li, Q. et al. Role of iodine recycling on sea-salt aerosols in the global marine boundary layer. *Geophys. Res. Lett.* **49**, e2021GL097567 (2022).
84. Du L. et al. Droplet surface spontaneous oxidation as a dominant formation pathway of organosulfates in the marine atmosphere. https://doi.org/10.5281/zenodo.16990475 (2025).

Acknowledgements

This work was supported by the National Key Research and Development Program of China (2023YFC3706203 (L.D.), 2023YFC3710400 (K.L.)), the National Natural Science Foundation of China (22376121 (L.D.), 22361162668 (L.D.)), the Intramural Joint Program Fund of State Key Laboratory of Microbial Technology (Project NO. SKLMTIJP-2025-02 (L.D.)), and the European Research Council (ERC) under the Horizon 2020 research and innovation program/ERC Grant Agreement 101052601—Spontaneous interfacial oxidant formation as a key driver for aerosol oxidation (SOFA) (C.G.).

Author contributions

All authors contributed extensively to the work presented in this paper. L.D., K.L., Y.R.S., and J.L.L. designed and performed the experiments, analyzed data, and drafted the paper. Y.R.S., Y.B.W., X.Q.M., Z.M.Y., J.H., K.Y.H., X.X.G., and Q.Y.L. performed the experiments and analyzed the data. H.Y., C.G., and M.F.G. reviewed the paper.

Competing interests

The authors declare no competing interests.

Additional information

Supplementary information The online version contains supplementary material available at https://doi.org/10.1038/s41467-025-65008-3.

Correspondence and requests for materials should be addressed to Lin Du or Kun Li.

Peer review information *Nature Communications* thanks the anonymous reviewer(s) for their contribution to the peer review of this work. A peer review file is available.